



OPEN ACCESS

EDITED BY

Kashif Mairaj Deen,
University of British Columbia, Canada

REVIEWED BY

Demian Ifeanyi Njoku,
Hong Kong Metropolitan University, China
Ameeq Farooq,
University of the Punjab, Pakistan

*CORRESPONDENCE

Aruliah Rajasekar,
✉ rajasekargood@gmail.com
Tabarak Malik,
✉ tabarak.malik@ju.edu.et

†PRESENT ADDRESS

Tabarak Malik, Department of Biomedical
Sciences, Institute of Health, Jimma
University, Jimma, Ethiopia

RECEIVED 11 October 2024

ACCEPTED 08 January 2025

PUBLISHED 14 February 2025

CITATION

Vignesh K, Sujithra S, Vajjiravel M, Santhosh S,
Narenkumar J, AlSalhi MS, Devanesan S,
Arunkumar P, Rajasekar A and Malik T (2025)
Structurally modified
tetrabromophthalic-based compounds as an
anti-corrosion agent in microbial influenced
saline systems.
Front. Mater. 12:1508966.
doi: 10.3389/fmats.2025.1508966

COPYRIGHT

© 2025 Vignesh, Sujithra, Vajjiravel, Santhosh,
Narenkumar, AlSalhi, Devanesan, Arunkumar,
Rajasekar and Malik. This is an open-access
article distributed under the terms of the
[Creative Commons Attribution License \(CC
BY\)](https://creativecommons.org/licenses/by/4.0/). The use, distribution or reproduction in
other forums is permitted, provided the
original author(s) and the copyright owner(s)
are credited and that the original publication
in this journal is cited, in accordance with
accepted academic practice. No use,
distribution or reproduction is permitted
which does not comply with these terms.

Structurally modified tetrabromophthalic-based compounds as an anti-corrosion agent in microbial influenced saline systems

Krishnan Vignesh¹, Sankar Sujithra², Murugesan Vajjiravel²,
Selvakumar Santhosh¹, Jayaraman Narenkumar³,
Mohamad S. AlSalhi⁴, Sandhanasamy Devanesan⁴,
Paulraj Arunkumar⁵, Aruliah Rajasekar^{1*} and Tabarak Malik^{6*†}

¹Environmental Molecular Microbiology Research Laboratory, Department of Biotechnology, Thiruvalluvar University, Vellore, Tamil Nadu, India, ²Department of Chemistry, School of Physical and Chemical Sciences, B S AbdurRahman Crescent Institute of Science and Technology, Chennai, India, ³Department of Biochemistry, Centre of Molecular Medicine and Diagnostics (COMManD), Saveetha Dental College and Hospitals, Saveetha Institute of Medical and Technical Sciences, Saveetha University, Chennai, India, ⁴Department of Physics and Astronomy, College of Science, King Saud University, Riyadh, Saudi Arabia, ⁵School of Chemical Engineering, Chonnam National University, Gwangju, Republic of Korea, ⁶Division of Research and Development, Lovely Professional University, Phagwara, Punjab, India

This study investigates the efficacy of synthesized corrosion inhibitors and evaluates them for microbial influenced corrosion (MIC) control in carbon steel API 5LX80 induced by *Pseudomonas aeruginosa* in 3.5 wt% NaCl. Tetrabromophthalic-based inhibitors (TBIs) have been synthesised and ascertained on the basis of spectral measurements determined by Fourier transform infrared spectroscopy (FTIR) and systematically evaluated for MIC. The results showed that this TBI effectively reduced biofilm formation at 200 ppm. FTIR and X-ray diffraction (XRD) observations confirmed that adsorption of a protective film over the surface of metal inhibited bacterial growth. FTIR analysis revealed the adhesion of the inhibitor over the metal surface. Polarization studies indicated that this inhibitor 1 decreased the corrosion current densities ($1.4588 \times 10^{-4} \text{A/cm}^2$) by a mixed-mode mechanism (both anodic and cathodic) and exhibited 75% corrosion inhibition efficiency. Thus, the present investigation has gained significance in reporting about novel corrosion inhibitors possessing biocidal activity to control MIC in API 5LX80 carbon steel used in oil and pipeline transporting properties.

KEYWORDS

Pseudomonas aeruginosa, microbial influenced corrosion, corrosion inhibitor, carbon steel API 5LX80, modified tetrabromophthalic compounds

Introduction

Microbial influenced corrosion (MIC), is a type of corrosion which is generally formed by the secretion of extracellular polymeric substances (EPS) by microorganisms, resulting

in a distraction caused by the microorganisms by producing a biofilm layer on the metal surface (Liu et al., 2018; Liu et al., 2016; Jia et al., 2017a). MIC was identified more than hundred years ago (Gaines, 1910). MIC often takes place in various environments, including gas and oil industries, marine settings, cooling water system (Jia et al., 2018a), and healthcare facilities. MIC is defined as the breakdown of metals induced by microbes like bacteria (Little et al., 2020), fungi (Rajasekar et al., 2009; Obot et al., 2009), and archaea, which exhibit a direct interaction with the surface of the metals. Through the development of biofilm layers, MIC may change the electrochemical conditions at the metal/solution interface (Salgar-Chaparro et al., 2020). According to estimates, MIC is liable for 20%–30% of all external corrosion issues and nearly 40% of interior corrosion issues in pipelines. Carbon steel has been highly used as pipeline materials in the gas and oil industries (Wolodko et al., 2018). A significant amount of MIC is caused by localized attacks, exhibiting extensive penetration into the base metal (Usher et al., 2014). Corrosion has serious negative impacts on the environment, human health, finances, and even a company's brand. Plans for managing industry risks and assessing equipment and facilities are put into place to protect them, but maintaining control over MIC is difficult due to its complexity and unpredictability. Since microorganisms were first linked to the corrosion process, several molecular mechanisms have been proposed (Li X. L. et al., 2018; Salgar-Chaparro et al., 2022). MIC mechanisms are generally classified into two predominant categories, namely, extracellular electron transfer MIC (EET-MIC), which occurs when microbial cells directly or indirectly take up the electron sources from the metallic material, and chemical MIC (CMIC), which arises from corrosive metabolites released by microbes during their metabolic activity (Su et al., 2020). Microorganisms can further accelerate the corrosion through other mechanisms or disrupt the protective layer on the surface of the metal (Dou et al., 2019). MIC has been associated with several types of microorganisms such as iron-oxidising bacteria (Wang et al., 2014; Liu et al., 2017), iron-reducing bacteria (Su et al., 2023), acid-producing bacteria (Gu, 2014), and sulphate-reducing bacteria (Jia et al., 2018b). Tetrabromo derivatives are increasingly recognized for their effectiveness as corrosion inhibitors, particularly in harsh environments like acidic and saline media. These compounds exhibit strong adsorption properties due to their higher electron density, which allows them to form stable protective films on the metal surface. The adsorption of tetrabromophthalic compounds shows potential to decrease the corrosion rate by inhibiting access to the active sites on the metallic surface, thus lowering the corrosion current and increasing the charge transfer resistance (R_{ct}) (Vignesh et al., 2024). Additionally, the halogen atoms in tetrabromo derivatives enhance the inhibition efficiency by promoting stronger chemical interactions with the metal, making them promising candidates for industrial corrosion protection (El-Aouni et al., 2023). For corrosion protection, inhibitors are used to reduce metal degradation, and they form protective barriers that prevent microorganisms from contacting the metal or inhibit the formation of biofilm (Li et al., 2024). In the present study, we develop the significant and cheapest alternative anti-corrosion agent to control severe biocorrosion. Hence, the TBI inhibitor was synthesised and employed as biocide to inhibit *Pseudomonas aeruginosa* biofilm formation on carbon

steel. Organic corrosion inhibitors are essential in many industrial applications for mitigating the detrimental effects of corrosion.

Materials and methods

Materials and reagents

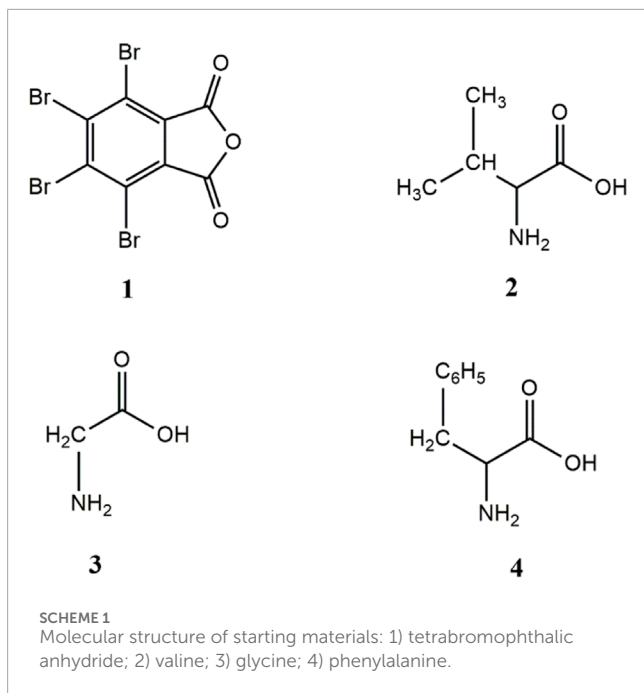
The starting materials, tetrabromophthalic anhydride (TBPA), and different amino acids such as glycine, valine, and phenylalanine were purchased from Sigma-Aldrich, India. Glacial acetic acid, ethanol, and acetone were used as the solvent, and reagents were obtained from TCI, Merck, and Avra Chemical Company from India. The Fourier transform infrared spectroscopy (FTIR) spectrum was recorded using an FTIR spectrometer (JASCO) in the region of 400–4000 cm^{-1} . The proton nuclear magnetic resonance (^1H NMR) spectrum was recorded with a Bruker 400 spectrometer using d-CHCl_3 as a solvent and TMS as the internal reference.

Synthesis of N-substituted tetrabromophthalic compounds (I–III)

The starting materials, name, and molecular structure of the synthesised compounds are given in Schemes 1, 2. The general synthetic pathway of compounds 01–03 is shown in Scheme 2. The procedure of the synthesis of compounds (01–03) was adopted from the reported literature and synthesized compound was shown in Scheme 3 (Tagle et al., 2015; Swathi et al., 2019). The calculated amount of TBPA (0.001 mol) was taken in a round-bottom (RB) flask with 30 mL of glacial acetic acid; then, it was stirred for approximately 30 min to dissolve TBPA in glacial acetic acid. A stoichiometric equivalent amount of 1) valine (0.1400 g, 0.001 mol), 2) glycine (0.1300 g, 0.001 mol), and 3) phenylalanine (0.1900 g, 0.001 mol) in glacial acetic acid was prepared. These solutions (amino acids) were added dropwise into the round-bottom (RB) flask containing a solution of TBPA. Then, the reaction mixture was stirred for 12 h under gentle reflux conditions. Finally, the reaction mixture was cooled, and acetic acid was removed under vacuum. The obtained solid was neutralized, filtered, and washed several times with water. The obtained compound was dried under vacuum, recrystallized, and then used for further investigation.

Bacterial strain and culture conditions

Previously isolated *P. aeruginosa* SKR10 from the wastewater of the industrial cooling tower by Kokilaramani et al. (2020) was used in this research project. The strain was identified through 16S rRNA sequencing and has been recorded in the NCBI GenBank with the accession number MT211518.1. The strain was retrieved from the glycerol stocks by subculture using the Luria-Bertani (LB) agar medium and incubated at 37°C for 24 h. A robust bacterial culture was then grown from a single colony in Luria-Bertani (LB) broth, which was placed in an orbital motion shaker with agitation at 150 rpm for 24 h at 37°C (Parthipan et al., 2021; Jia et al., 2017b).



Well diffusion method

The antibacterial study of the synthesised inhibitor against the corrosion-inducive bacteria *P. aeruginosa* SKR10 was determined using the agar diffusion technique (Jung et al., 2022). Mueller Hinton Agar (Himedia) was used to determine the antimicrobial activity of the three synthesised inhibitors (In 1-TB-1,3-DOIBA, In 2-TB1,3DOIAA, and In 3-TB1,3DOIPA) and was added to the individual well at various concentrations (50, 100, 150, and 200 ppm) (Li Y. et al., 2018). The negative/positive control of this experiment was performed using deionised water and gentamycin. After 24 h of treatment, the average diameter of the inhibition zone surrounding the disc was measured using a ruler in millimetres (mm) to assess the toxicity.

Biofilm inhibitory assay

To determine the biofilm inhibitory effects of synthetic corrosion inhibitors (In - TB-1,3-DOIBA, In 2 - TB1,3DOIAA, and In 3 - TB1,3DOIPA) by the corrosion-causing bacterium *P. aeruginosa* SKR10, the bacterial isolates of interest were cultured in LB broth medium, followed by a 24-h incubation period at 37°C. The cultures were diluted to achieve a specific optical density (OD⁶⁰⁰) of 0.1, which corresponds to approximately 1×10^8 CFU/mL (Lee et al., 2024). Further dilution achieved a final concentration of 1×10^6 CFU/mL for biofilm formation assays. The suppression of biofilm development was assessed using a microtiter plate method; sterile polystyrene microtiter plates were filled with the bacterial suspension along with different concentrations of the inhibitors (50 ppm, 100 ppm, and 200 ppm) (Narenkumar et al., 2016). Control wells contained the same culture broth without inhibitors; the sterile 96-well plate was incubated at 37°C for 24 h, and the suspended growth medium was removed; then, the

plates were washed using PBS, and after removing the suspended growth media, PBS was used to wash the sterile 96-well plate. Subsequently, 120 μ L of the crystal violet solution was added to each well, and they were left to stand for 20 min. Following this, 125 μ L of acetic acid was added to each well, and the mixture was then incubated for further 15 min at 37°C. Finally, the amount of biofilms produced was measured using a microplate reader at an absorbance of 595 nm (Ibrahim et al., 2022).

Coupon preparation

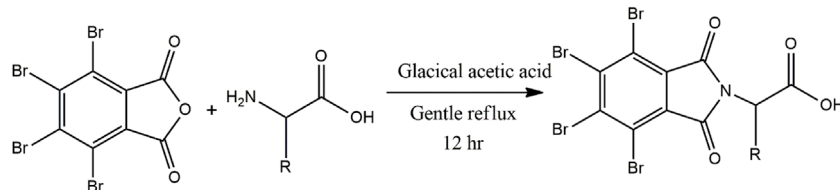
In this study, API 5LX80 carbon steel was used to evaluate MIC. The chemical composition of API 5LX80 is as follows (wt%): Cr, 0.03; C, 0.070; Ni, 0.02; Al, 0.029; Cu, 0.05; Mn, 1.05; and Si, 0.195, balanced with Fe suspension. The rectangular coupons have a 1 cm² exposed surface area, which is utilized for electrochemical impedance spectroscopy (EIS) and Tafel polarization. Similarly, 2.5 cm² was used for weight loss analysis (Abdallah et al., 2018). All the specimens were polished with 600, 800, 1,000, and 1,200 grit of silicon carbide metallurgical paper; the polished specimens were thoroughly rinsed with Milli-Q water, degreased in acetone, and dried in a nitrogen gas stream before storing it in a desiccator until further use; then, the coupons were weighed and exposed to 15 min of ultraviolet (UV) light before immersion (Parthipan et al., 2017; Katara et al., 2008).

Weight loss analysis

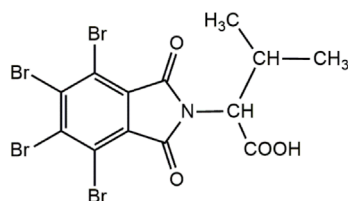
The initial weight of the triplicated coupons was recorded prior to immersion in the corrosive solution of 3.5 wt.% NaCl. In order to calculate the weight elimination of those corrosion systems that were carried out in triplicate, the carbon steel API 5LX80 coupons were placed on a 500-mL conical flask containing 400 mL of 3.5 wt.% NaCl medium. System 1 acts on abiotic control, and system 2 acts on biotic control with the *P. aeruginosa* SKR10 inoculum (approximately 10^4 CFU/mL). Systems 3, 4, and 5 were added with 200 ppm of inhibitors. Similarly, systems 6, 7, and 8 were added with 200 ppm of inhibitors and additionally inoculated with *P. aeruginosa* SKR10 at a concentration of approximately 2.2×10^6 CFU/mL (Kokilaramani et al., 2022). These corrosion systems were maintained at an identical temperature of 37°C for 7 days without any interruptions. The coupons were acquired and subsequently subjected to pickling treatment in Clark's solution, consisting of 5% of stannous chloride and 2% antimony trioxide dissolved in concentrated hydrochloric acid (HCl) with continuous agitation at room temperature for 5–10 min, prior to being rinsed with double-distilled water and dried with an air dryer (Rajasekar et al., 2011). Finally, all coupons' weight was recorded, and the corrosion rates (Equation 1) were determined in accordance with the standards provided by the National Association of Corrosion Engineers.

Equation 1 is expressed as follows:

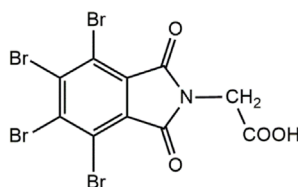
$$\text{Corrosion Rate (mmy)} = \frac{K * Wl(g)}{D\left(\frac{g}{cm^2}\right) * A(cm^2) * T(hrs)}, \quad (1)$$



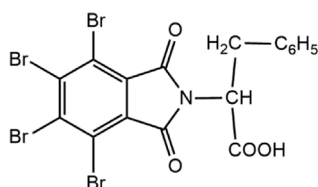
SCHEME 2
General representation of the synthesis of compounds: I–III.



Compound: 01: TB-1, 3-DOIBA: 3-methyl-2-(4, 5, 6, 7-tetrabromo-1, 3-dioxoisindolin-2-yl) butanoic acid



Compound: 02: TB1, 3DOIAA: 2-(4, 5, 6, 7-tetrabromo-1, 3-dioxoisindolin-2-yl) acetic acid



Compound: 03: TB1, 3DOIPA: (S)-3-phenyl-2-(4, 5, 6, 7-tetrabromo-1, 3-dioxoisindolin-2-yl) propanoic acid

SCHEME 3
Molecular structure of synthesized compounds I–III.

where $K = 8.76 \times 10^4$; W_l = weight loss (g); mmy = corrosion rate (millimetre per year penetration); D = density of metal (g/cm^3); A = exposure area (cm^2); T = exposure time in a corrosive environment (hrs).

Electrochemical measurements

The electrochemical analyses, including electrochemical impedance spectroscopy (EIS) and polarization studies, were conducted using the Metrohm Autolab instrument (PGSTAT204),

Netherlands, coupled with Nova 2.1.7 software. All the electrochemical analyses were performed under a conventional three-electrode configuration assembly: the reference electrode was Ag/AgCl (3M KCl), the working electrode was composed of API 5LX80 carbon steel coupon, and platinum mesh was used as the counter electrode. EIS was performed at the open-circuit potential (OCP) using a 10 mV sinusoidal voltage signal with a frequency range of 10^{-2} – 10^5 Hz (Wang et al., 2018), employing a scanning rate of 0.010 V/min (Liu et al., 2015). Potentiodynamic polarization analysis was performed: anodic polarization up to +200 mV and cathodic polarization down to –200 mV were

executed at a scanning rate of 0.002 V/s relative to the corrosion potential (E_{corr}).

Fourier transform infrared spectroscopy analysis

To confirm the functional constituents, the corrosion product was collected after the weight loss measurement study. The corrosion product was adequately dried and kept in the desiccated specimens were homogenized with potassium bromide (KBr) to create pellets of uniform shape and composition. The pellets were subjected to FT-IR spectroscopy (Version 10.6.0 of the PerkinElmer Spectrum IR) analysis within the wave number of 400–4,000 cm^{-1} , employing an 8 cm^{-1} resolution and conducting 64 scans per spectrum to achieve comprehensive characterization (Kashyap et al., 2022).

X-ray diffraction analysis

The carbon steel API 5LX80 corrosion products from the systems S1 to S8 were subjected to XRD analysis using a Bruker D8 instrument equipped with a LynxEye and scintillation counter detector. The analysis spanned an angular range of 5–140°, with X-ray tube settings at 40-kV and 30-kV power levels (Muthukrishnan et al., 2017).

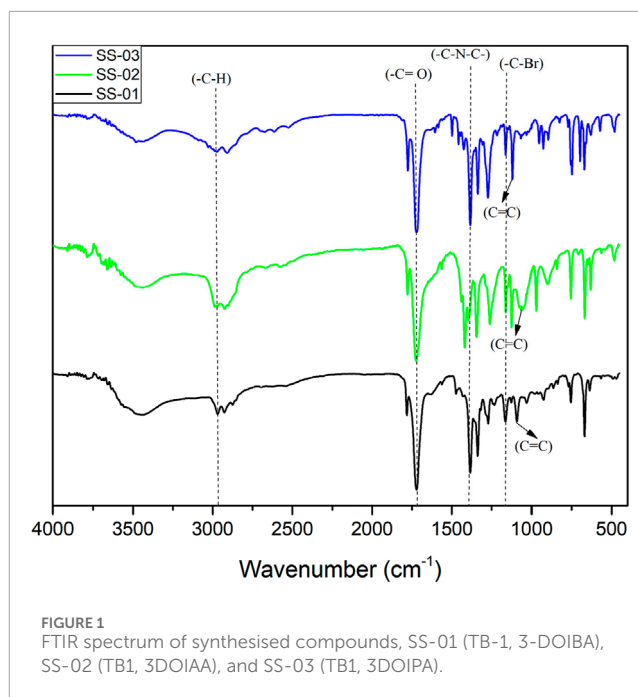
Results and discussion

Fourier transform infrared spectroscopy analysis of synthesised compounds

The FTIR spectra of synthesised compounds are shown in Figure 1: I: 3-methyl-2-(4, 5, 6, 7-tetrabromo-1, 3-dioxoisindolin-2-yl) butanoic acid (TB-1, 3-DOIBA); II: 2-(4, 5, 6, 7-tetrabromo-1, 3-dioxoisindolin-2-yl) acetic acid (TB1, 3DOIAA); and III: (S)-3-phenyl-2-(4, 5, 6, 7-tetrabromo-1, 3-dioxoisindolin-2-yl) propanoic acid (TB1, 3DOIPA); compound functional groups and their relevant stretching frequencies are presented in Table 1.

Well diffusion method

The antibacterial activities of the synthesized inhibitors (TB-1,3-DOIBA, TB1,3DOIAA, and TB1,3DOIPA) assessed using the well diffusion technique at various concentrations (50, 100, 150, and 200 ppm) were tested. The synthesised inhibitors showed the highest zones of inhibition observed at an optimum concentration of 200 ppm at 2.92 ± 0.1 mm, 2.31 ± 0.1 mm, and 0.92 ± 0.1 mm in TB-1,3-DOIBA, TB1,3DOIPA, and TB1,3DOIAA, respectively. The inhibitors were extremely efficient against the *P. aeruginosa* SKR10 bacteria at 200 ppm of TB-1,3-DOIBA and TB1,3DOIPA, which suppressed the bacterial growth rate in a random manner over other concentrations (Kokilaramani et al., 2021).



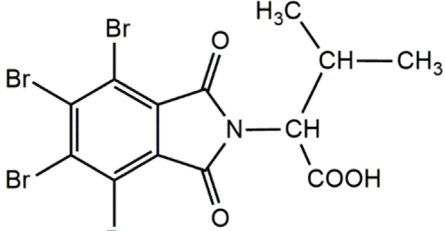
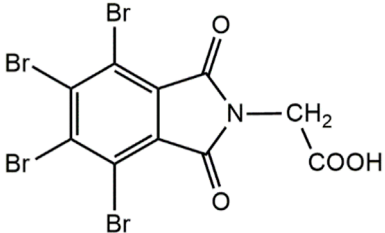
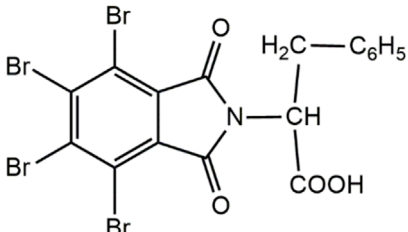
Biofilm inhibitory assay

The biofilm assay of TBI synthesised inhibitors at various concentrations of 50, 100, and 200 ppm was chosen to assess the biofilm inhibition efficiency against strain *P. aeruginosa* SKR10 with the crystal violet method. The inhibition efficiencies of inhibitors 1 to 3 were 79.6%, 42.7%, and 71%, respectively. As illustrated in Figure 2, the inhibitors significantly reduced the biofilm growth on well surfaces at the optimum concentration of 200 ppm. The prominent violet colour variations in the wells reveal the biofilm's retention of the crystal violet dye, which are due to the extensive stacking of biofilm structures. This occurrence demonstrates the potential of inhibitors to inhibit the formation of EPS, such as proteins, lipids, and carbohydrates (Qi et al., 2024). This inhibition of EPS production was crucial as these substances play a vital role in the formation of biofilm and stability. Hence, the ability of inhibitors to disrupt EPS production indicated a possibility for inhibiting biofilm efficiencies. Based on the biofilm assay, all the three inhibitors were further chosen for biocorrosion evaluation of carbon steel API 5LX80.

Weight loss analysis

In order to describe the corrosion behaviour of carbon steel API 5LX80 induced by strain *P. aeruginosa* SKR10, the average corrosion rates and the weight loss of specimens with and without the presence of *P. aeruginosa* and the inhibitors were determined from the obtained weight loss experiment results. Table 2 shows the specimens' weight loss and corrosion rates during a 7-day period with and without the presence of *P. aeruginosa* SKR10, and Figure 3 shows before and after immersion of carbon steel API 5LX80. In the abiotic and biotic systems, S1 and S2 exhibit

TABLE 1 FTIR spectrum results of synthesised compounds.

Molecular structure and code	Functional group	Assigned stretching frequency (cm ⁻¹)
 TB-1, 3-DOIBA	-C-Br group (aromatic)	1,093 and 1,163
	-C=O group	1,715
	-C-N-C	1,267
	Aromatic ring: C=C; =C-H (stretch, sp ²)	1,382; 2,969
	Acidic group: (O-H); (C=O)	3,463 and 1781
 TB1, 3DOIAA	-C-Br group (aromatic)	1,058 and 1,123
	-C=O group	1,716
	-C-N-C	1,263
	Aromatic ring: C=C; =C-H (stretch, sp ²)	1,418; 2,984
	Acidic group: (O-H); (C=O)	3,468 and 1,781
 TB1, 3DOIPA	-C-Br group (aromatic)	1,118 and 1,163
	-C=O group	1,722
	-C-N-C	1,267
	Aromatic ring: C=C; =C-H (stretch, sp ²)	1,382; 2,969
	Acidic group: (O-H); (C=O)	3,478 & 1,781

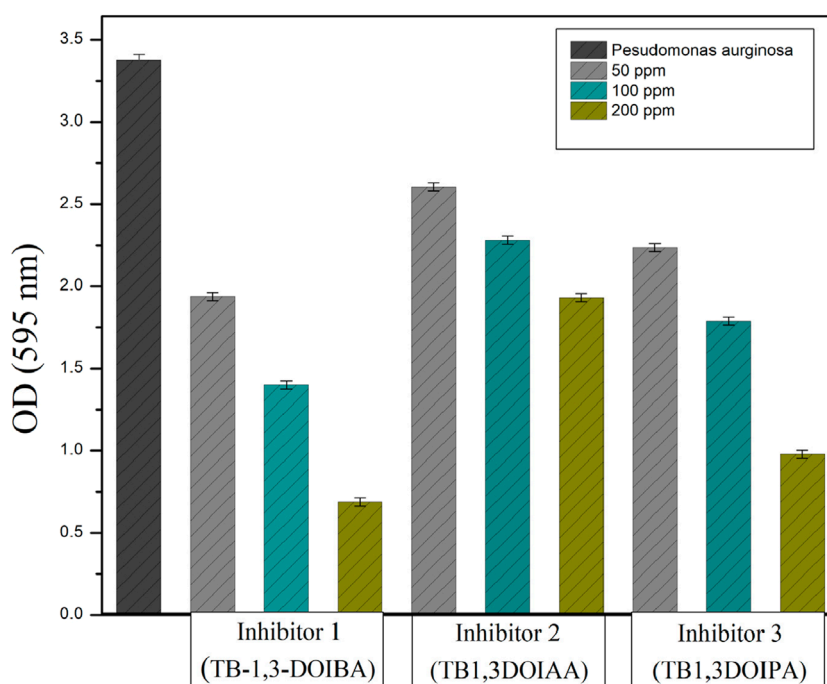


FIGURE 2
Biofilm assay of *P. aeruginosa* in the presence of inhibitors at various concentrations.

TABLE 2 Weight loss analysis of carbon steel API 5LX80 in the presence and absence of *P. aeruginosa* and inhibitors. S1—Abiotic, S2—Biotic, S3—Inhibitor 1, S4—Inhibitor 2, S5—Inhibitor 3, S6—*P. aeruginosa* with S3, S7—*P. aeruginosa* with S4, and S8—*P. aeruginosa* with S5.

System	Average weight loss (mg)	Corrosion rate (mm/y)	Inhibition efficiency [IE (%)]
S1	74.9 ± 1.5	4.95 ± 0.1	—
S2	96.2 ± 0.5	6.36 ± 0.1	—
S3	18.8 ± 1.5	1.25 ± 0.1	75
S4	38.2 ± 0.5	2.52 ± 0.1	49
S5	28.8 ± 2.0	1.91 ± 0.1	61
S6	36.7 ± 1.5	2.43 ± 0.1	62
S7	54.2 ± 0.5	3.58 ± 0.1	44
S8	46.0 ± 2.0	3.04 ± 0.1	52

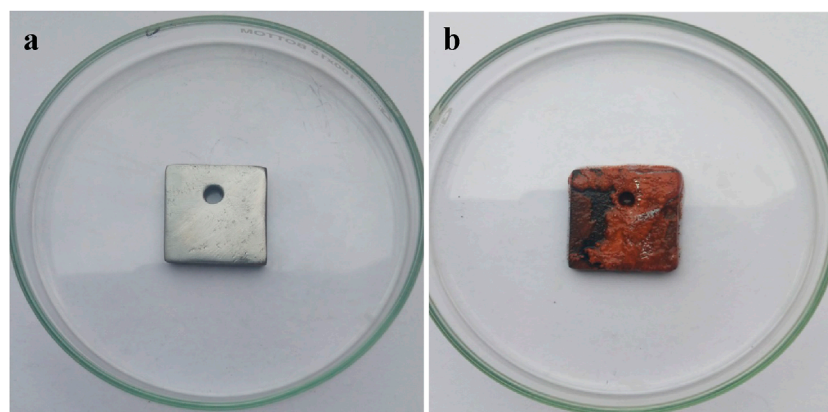


FIGURE 3 Image shows the carbon steel API 5LX80 coupons after the corrosion studies at a period of 7 days. (A) Before immersion. (B) After 7 days of immersion.

74.9 ± 1.5 mg and 96.2 ± 0.5 mg, respectively. These results represent that *P. aeruginosa* SKR10 exhibited 22.1% ± 0.2% more weight loss compared with the abiotic system. In the presence of inhibitors in experimental systems, S3 to S5 showed 18.8 ± 1.5, 38.2 ± 0.5, and 28.8 ± 2.0 mg, respectively, followed by the corrosion rates of 1.25 ± 0.1, 2.52 ± 0.1, and 1.91 ± 0.1 mm/year, respectively. However, in the presence of inhibitors with *P. aeruginosa* SKR10 presenting S6–S8, these systems showed 36.7 ± 1.5, 54.2 ± 0.5 mg, and 46 ± 2.0 mg weight loss were observed, followed by the corrosion rates recorded as 2.43 ± 0.1, 3.58 ± 0.1, and 3.04 ± 0.1 mm/year, respectively. Moreover, the inhibitor has the efficiency to inhibit biofilm formation and thus reduce the corrosion rate, which are related to the MIC (Idelfitri et al., 2023; Azzouzi et al., 2022). Among the inhibitors, inhibitors 1 and 3 exhibited the effective inhibition efficiencies of 75% and 61%, respectively. Overall, weight loss results underscore the potential of inhibitors for mitigating corrosion and also reducing the MIC.

Electrochemical impedance spectroscopy

Electrochemical impedance spectroscopy (EIS) was used to analyse the electrochemical characteristics of surfaces subjected to corrosion after exposure of both sterile and bacteria-inoculated media. Figure 4 shows the EIS graphical representation of API 5LX80 carbon steel with and without the presence of inhibitors and *P. aeruginosa* SKR10. Figure 4A represents a Nyquist plot, and Figure 4B represents a bode plot of the EIS properties. ZView software (version 3.0) was used to find a suitable equivalent circuit for each system and obtain the best fitting of each data with their corresponding equivalent circuits (AlSalhi et al., 2023); these models are shown in Figure 5. The surface roughness capacitance of the working electrode is determined using a model involving a constant phase element (CPE), and the electrochemical impedance spectroscopy (EIS) values, including charge transfer resistance (R_{ct}) and solution resistance (R_s), for the various systems are shown in Table 3. The abiotic system S1 R_{ct} is observed as 92.221 Ω

cm², followed by the biotic system *P. aeruginosa* SKR10 inoculated S2 slightly decreased as 78.52 Ω cm². The highest R_{ct} values were observed in system S3 containing the inhibitor TB-1,3-DOIBA showing the value 201.47 Ω cm², and systems S4 and S5 containing inhibitors TB1,3DOIAA and TB1,3DOIPA show values 153.13 Ω cm² and 167.4 Ω cm², respectively. The *P. aeruginosa* SKR10 bacterium possessed the inhibitor systems S6–S8, and their R_{ct} values were 101.96 Ω cm², 81.063 Ω cm², and 94.843 Ω cm², respectively. In the presence of bacteria and inhibitor (S6–S8), the Z-value was increased by exposure time and reached its highest amount after the end of the exposure (Figure 4A). The bode-phase plots of carbon (Figure 4B) show one peak maxima in media after the end of the exposure at the low and high frequency ranges, representing the inhibition of biofilm on the metal surface. The higher R_{ct} values were observed in inhibitor systems with and without bacteria, confirming that the synthesised inhibitors were adsorbed on the metallic surface to form a thick protective layer and thus reduce the corrosion rate (Narenkumar et al., 2019). The formation of the protective layer occurred through electron transfer between phases, specifically from the electrode to hydrogen ions in the aqueous phase influenced by the resistance of the metal surface.

By specifying the values of R_{ct}, the surface coverage (θ) and inhibition efficiency (η%) parameters were calculated from the following Equation 3 (Majidi et al., 2019):

$$\theta = \left(\frac{R_{Ct}^{(inhibitor)} - R_{Ct}^{(Control)}}{R_{Ct}^{(inhibitor)}} \right), \quad (2)$$

$$\eta\% = \theta \times 100. \quad (3)$$

In Equation 2, R_{Ct}^(Control) and R_{Ct}^(inhibitor) represent the charge transfer resistance in the absence and presence of inhibitors, respectively.

Tafel polarization

Figure 6 represents the polarization curves for API 5LX80 with and without bacteria and inhibitor at 7 days of immersion, and its associated data corrosion current (*i*_{corr}) and corrosion potential (*E*_{corr}) are presented in Table 4. In the biotic medium, the corrosion current was observed as 6.6716 × 10⁻⁴ A/cm², which confirms that *P. aeruginosa* SKR10 exhibits the highest potential for causing metal deterioration in a 3.5 wt% NaCl environment. However, in addition to the inhibitor medium, S3–S8 showed 1.4588 × 10⁻⁴ A/cm², 3.7175 × 10⁻⁴ A/cm², 1.9626 × 10⁻⁴ A/cm², 2.7313 × 10⁻⁴ A/cm², 5.2318 × 10⁻⁴ A/cm², and 4.0104 × 10⁻⁴ A/cm², respectively. In the presence of *P. aeruginosa* SKR10, *E*_{corr} shifted negatively and *i*_{corr} increased; this indicates that the cathodic reaction takes place, thus accelerating the corrosion by *P. aeruginosa* SKR10. The polarization measurement also revealed the higher oxidation rate of carbon steel in the S2 medium, which induced the acceleration of oxygen reduction and consequently increased the corrosion rate. The enzymatic processes of *P. aeruginosa* SKR10 utilize oxygen as the terminal electron acceptor and oxidize Fe through metabolic hydrogen peroxide by the catalase enzyme (Moradi et al., 2024). On the contrary, the significant increase in the oxidized species (Fe²⁺ and Fe³⁺) amount examined by XRD confirms that the electrons are essential for the growth and activity of bacteria

(Wang et al., 2022; Batmanghelich et al., 2017). Conversely, in the presence of an inhibitor, the *i*_{corr} value lower than the biotic medium, indicating inhibitor adsorption on the metal surface, led to the suppression of both anodic and cathodic reactions of corrosion (Pinnock et al., 2018; Rajput et al., 2021). Consequently, the inhibition efficiency of TBI was observed as approximately 74%, which indicated TBI as an excellent corrosion inhibitor for API 5LX80.

The surface coverage (θ) and inhibition efficiency (η%) parameters were calculated from the following Equation 5 (Majidi et al., 2019):

$$\theta = \left(\frac{i_{corr}^{(Control)} - i_{corr}^{(inhibitor)}}{i_{corr}^{(Control)}} \right), \quad (4)$$

$$\eta\% = \theta \times 100. \quad (5)$$

In Equation 4, *i*_{corr}^(Control) and *i*_{corr}^(inhibitor) represent the corrosion current density in the absence and presence of inhibitors, respectively.

Surface analysis

Fourier transform infrared spectroscopy analysis

The functional groups of the corrosion products and the findings of the inhibitor absence and presence on the metallic surface were identified using FTIR spectroscopy, as illustrated in Figure 7. The FTIR spectrum indicates the inhibitor binds with the API 5LX80 carbon steel metallic surface. The presence of the organic functional groups in the biocorrosion products was validated from the peaks, as observed in Figure 7. Among the peaks observed in the spectra, the peaks at 3,361 cm⁻¹ and 2,922 cm⁻¹ due to the stretching vibrations of -OH (hydroxyl) and -C-H (aliphatic group), respectively, indicating the presence of hydrophilic functionalities that can form hydrogen bonds with water or other molecules and -C-H groups, suggests the presence of organic compounds that may enhance corrosion resistance by creating a hydrophobic barrier, reducing water or ion penetration onto the metal surface. The absorption peak at 1,638 cm⁻¹ related to the stretching frequency carbonyl group (C=O) confirms that the carboxylic acid group is present in the corrosion products, suggesting its role in corrosion protection by forming complexes or chelates with metal ions (Vignesh et al., 2024). The signals for the stretching vibrations of -C-N-C-, -C=C (alkene), and -C-Br (aromatic halides) at different regions were observed at 1,387 cm⁻¹, 1,106 cm⁻¹, and 606 cm⁻¹ respectively; the -C-N-C- groups enhance barrier properties through hydrogen bonding, the -C=C groups increase structural rigidity, and the -C-Br groups provide hydrophobic characteristics to protect the metal surface (Sethi et al., 2013). A comparison of S3, S4, S5, S6, S7, and S8 and the inhibitor's functional groups indicates alterations upon the interaction with the metal surface, providing solid evidence of the binding of inhibitor components to the carbon steel API 5LX80 metal surface and subsequent suppression of biofilm development.

X-ray diffraction analysis

The XRD analyses of the corrosion products on API 5LX80 carbon steel with and without bacteria and inhibitor are presented

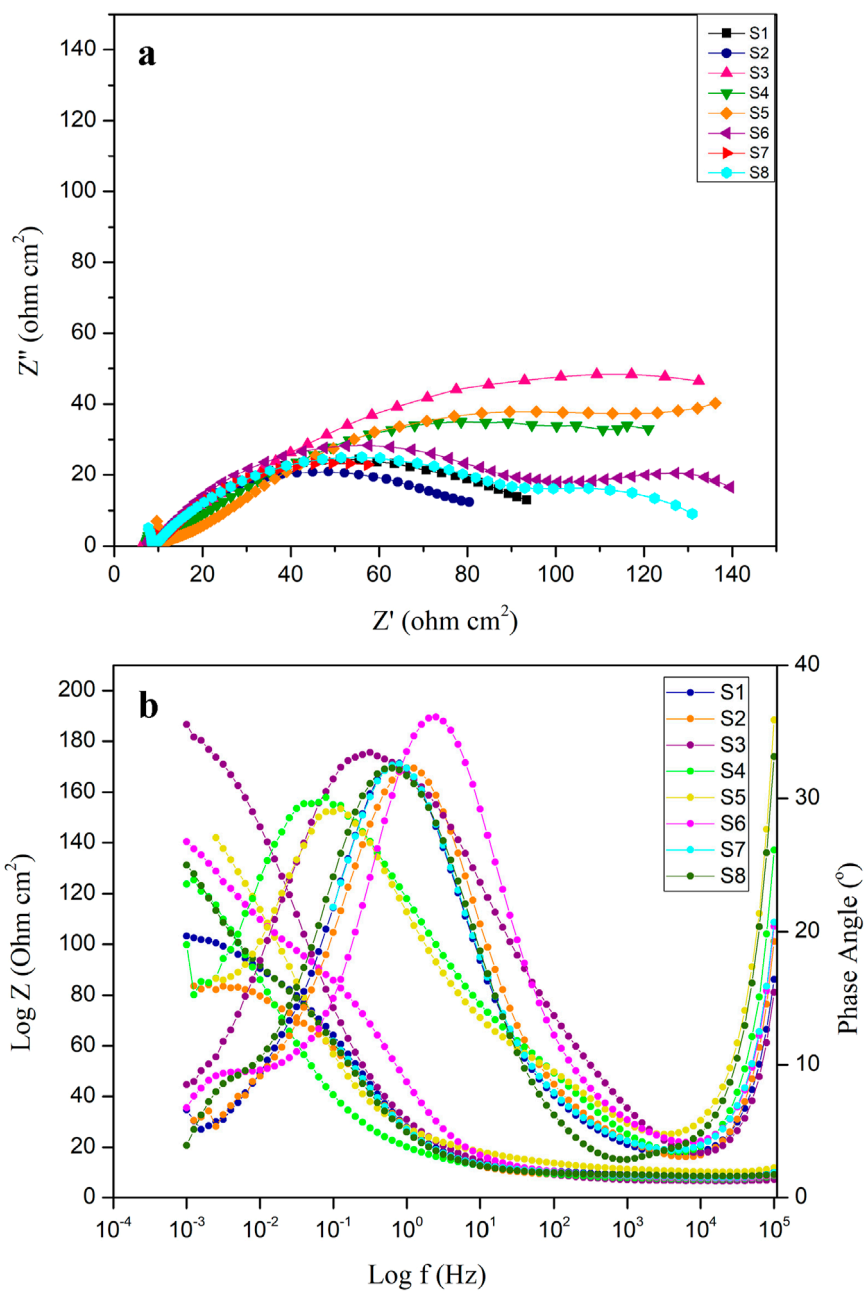


FIGURE 4 (A) Nyquist plot of carbon steel API 5LX80 after the corrosion studies. (B) Bode plot of carbon steel API 5LX80 after the corrosion studies. S1—abiotic, S2—biotic, S3—inhibitor 1, S4—inhibitor 2, S5—inhibitor 3, S6—*P. aeruginosa* with S3, S7—*P. aeruginosa* with S4, and S8—*P. aeruginosa* with S5.

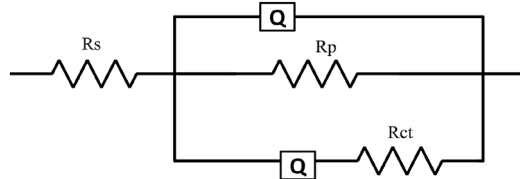


FIGURE 5 EIS circuit of the biocorrosion system.

in Figure 8. XRD analysis confirmed the formation of iron oxide-hydroxide JCPDS 01-089-5894, manganese oxide JCPDS 01-075-0826, and ferric oxide JCPDS 01-086-0551 corrosion products (Sun et al., 2016). The biotic systems indicated more strong peaks when compared to abiotic control; the iron particles found in the bacterial systems as corrosion products suggest that the bacterial strains are capable of oxidizing inorganic compounds included in the composition of carbon steel. The inhibitor-treated samples demonstrated reduced peak intensities, indicating that the inhibitors effectively suppressed

TABLE 3 Electrochemical impedance spectroscopy (EIS) parameters of carbon steel API 5LX80 in the presence and absence *P. aeruginosa* and inhibitors. S1—Abiotic, S2—Biotic, S3—Inhibitor 1, S4—Inhibitor 2, S5—Inhibitor 3, S6—*P. aeruginosa* with S3, S7—*P. aeruginosa* with S4, and S8—*P. aeruginosa* with S5.

System	CPE (F)	R_{ct} ($\Omega\text{ cm}^2$)	R_s ($\Omega\text{ cm}^2$)	n	θ	$\eta\%$
S1	$1.36 \times 10^{-2} \pm 0.1$	92.2 ± 2.0	9.22 ± 0.1	0.62 ± 0.01	—	—
S2	$1.19 \times 10^{-2} \pm 0.1$	78.5 ± 1.8	8.37 ± 0.1	0.62 ± 0.01	—	—
S3	$3.19 \times 10^{-2} \pm 0.1$	201.4 ± 3.5	9.15 ± 0.1	0.56 ± 0.01	0.54 ± 0.02	54 ± 0.2
S4	$1.43 \times 10^{-1} \pm 0.1$	153.1 ± 3.0	9.79 ± 0.1	0.54 ± 0.01	0.39 ± 0.02	40 ± 0.1
S5	$6.55 \times 10^{-2} \pm 0.1$	167.4 ± 2.5	14.37 ± 0.1	0.54 ± 0.01	0.44 ± 0.02	45 ± 0.1
S6	$4.22 \times 10^{-3} \pm 0.1$	101.9 ± 2.0	8.39 ± 0.1	0.65 ± 0.01	0.22 ± 0.02	23 ± 0.1
S7	$1.31 \times 10^{-2} \pm 0.1$	81.0 ± 2.0	9.96 ± 0.1	0.67 ± 0.01	0.03 ± 0.01	3 ± 0.1
S8	$1.69 \times 10^{-2} \pm 0.1$	94.8 ± 2.0	8.91 ± 0.1	0.62 ± 0.01	0.17 ± 0.02	17 ± 1

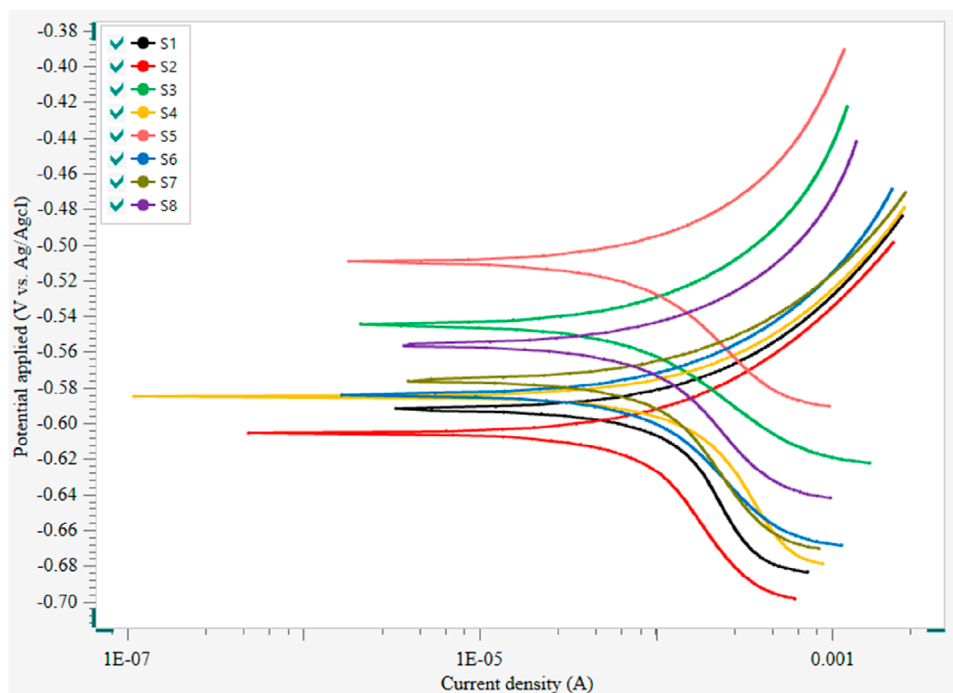


FIGURE 6 Tafel Polarization of carbon steel API 5LX80 after the corrosion studies. S1—abiotic, S2—Biotic, S3—inhibitor 1, S4—inhibitor 2, S5—inhibitor 3, S6—*P. aeruginosa* with S3, S7—*P. aeruginosa* with S4, and S8—*P. aeruginosa* with S5.

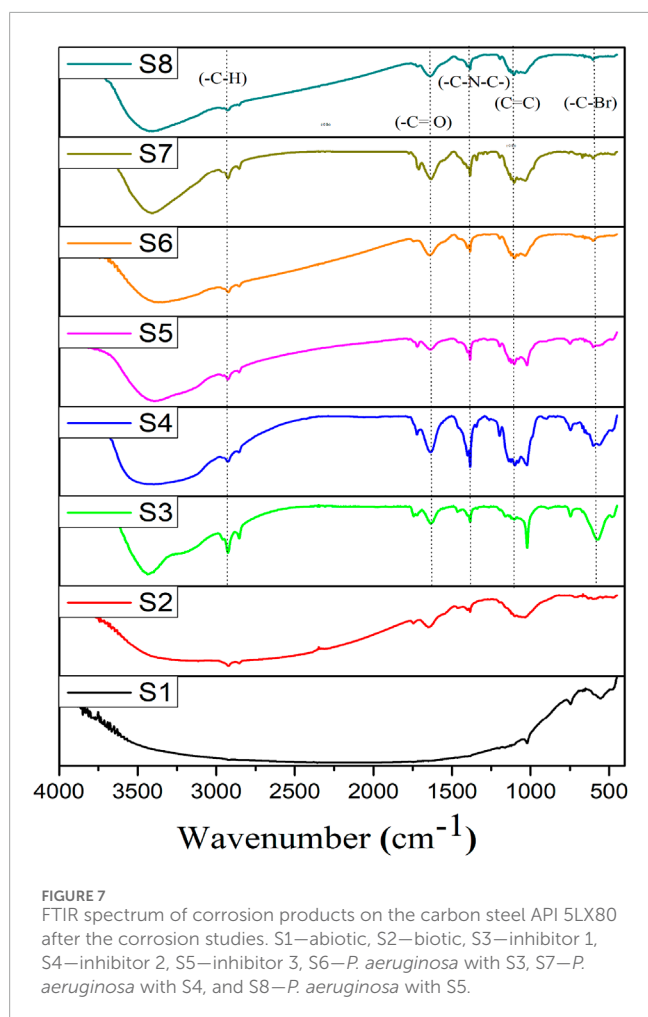
the formation of corrosion products, although some variation was noted. Notably, samples treated with both inhibitors with bacteria exhibited the lowest-intensity peaks comparable to those observed in the inhibitor systems, which suggested that the inhibition effects were maintained even in the presence of bacteria (Sachan and Singh, 2020). These findings of XRD analysis indicated that the inhibitor not only inhibits the growth of bacterial strain but also reduces the corrosion rate, most likely via adsorbing on the metal surface.

Proposed mechanism of inhibition of biocorrosion of carbon steel API 5LX80

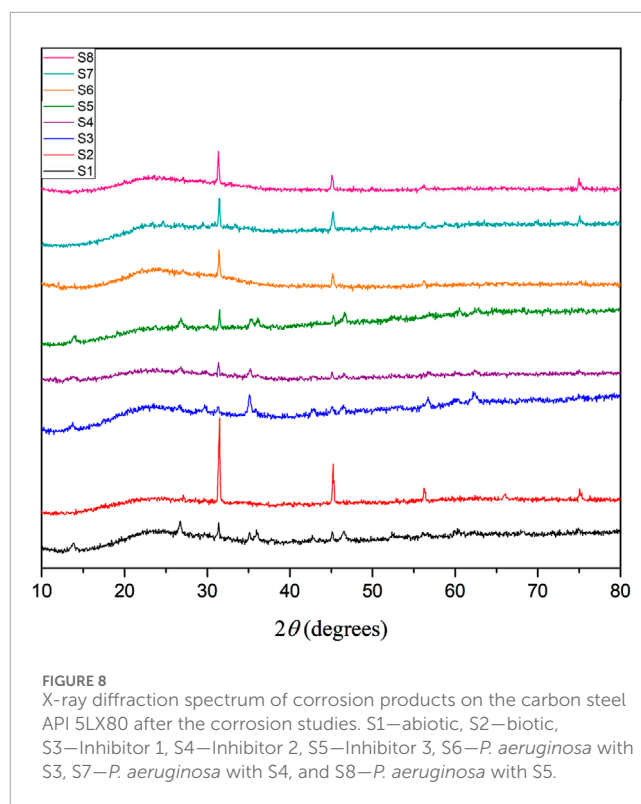
The biofilm inhibitory assay demonstrated that the bacterial strain exhibited high sensitivity to the synthesised inhibitor. This finding was further confirmed by linear polarization, EIS, FTIR, and XRD analyses conducted on bacterial systems with inhibitors. FTIR results show that inhibitor molecules attach to the metal surface via various organic functional groups found in corrosion products. These peaks correspond to the stretching vibrations of hydroxyl and aliphatic

TABLE 4 Tafel polarization parameters of carbon steel API 5LX80 in the presence and absence of *P. aeruginosa* and inhibitors. S1—Abiotic, S2—Biotic, S3—Inhibitor 1, S4—Inhibitor 2, S5—Inhibitor 3, S6—*P. aeruginosa* with S3, S7—*P. aeruginosa* with S4, and S8—*P. aeruginosa* with S5.

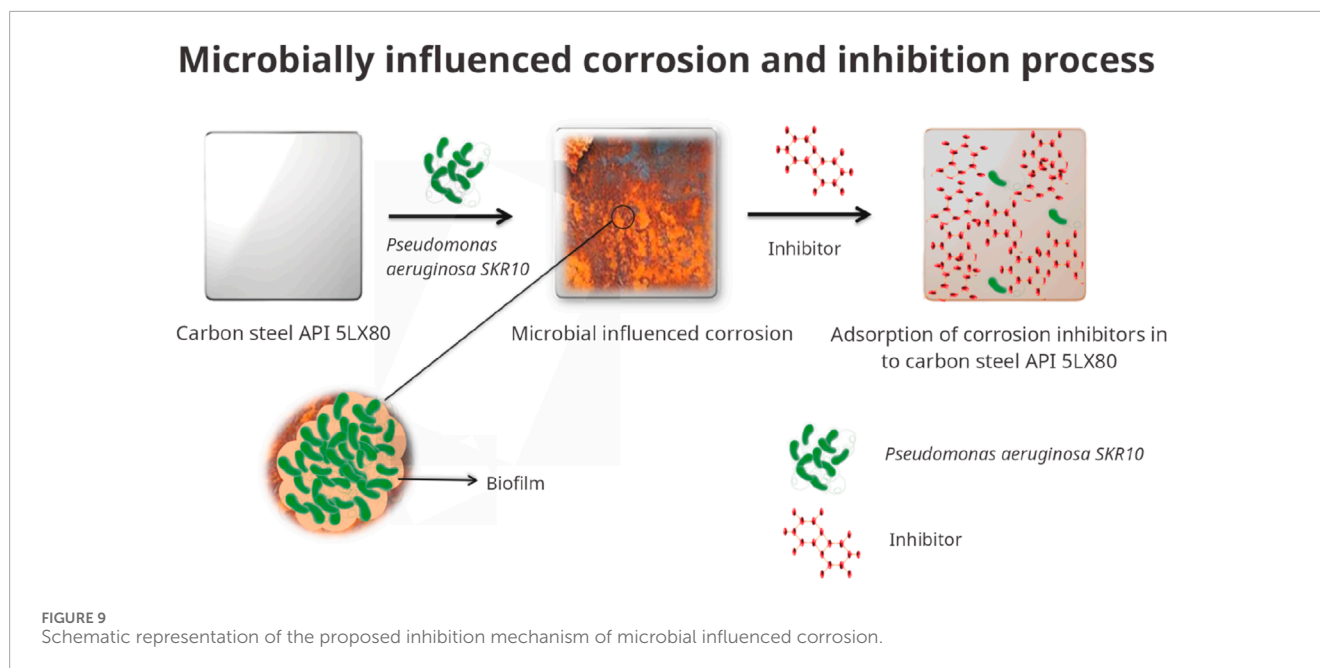
System	i_{corr} (A/cm ²)	E_{corr} (V)	b_a (V/dec)	b_c (V/dec)	Corrosion rate (mm/year)	θ	$\eta\%$
S1	$6.28 \times 10^{-4} \pm 0.1$	$-5.92 \times 10^{-1} \pm 0.01$	0.12 ± 0.01	-0.38 ± 0.01	5.13 ± 0.2	—	—
S2	$6.67 \times 10^{-4} \pm 0.1$	$-6.05 \times 10^{-1} \pm 0.01$	0.12 ± 0.01	-0.25 ± 0.01	6.43 ± 0.1	—	—
S3	$1.45 \times 10^{-4} \pm 0.1$	$-5.44 \times 10^{-1} \pm 0.01$	0.08 ± 0.01	0.14 ± 0.01	1.19 ± 0.1	0.76 ± 0.01	76 ± 0.5
S4	$3.71 \times 10^{-4} \pm 0.1$	$-5.84 \times 10^{-1} \pm 0.01$	0.10 ± 0.01	0.58 ± 0.01	2.31 ± 0.1	0.40 ± 0.01	41 ± 0.3
S5	$1.96 \times 10^{-4} \pm 0.1$	$-5.09 \times 10^{-1} \pm 0.01$	0.09 ± 0.01	0.27 ± 0.01	1.58 ± 0.2	0.68 ± 0.01	69 ± 0.4
S6	$2.73 \times 10^{-4} \pm 0.1$	$-5.84 \times 10^{-1} \pm 0.01$	0.09 ± 0.01	1.09 ± 0.01	2.54 ± 0.2	0.59 ± 0.01	59 ± 0.5
S7	$5.23 \times 10^{-4} \pm 0.1$	$-5.76 \times 10^{-1} \pm 0.01$	0.10 ± 0.01	-0.59 ± 0.01	3.71 ± 0.1	0.21 ± 0.01	22 ± 0.3
S8	$4.01 \times 10^{-4} \pm 0.1$	$-5.56 \times 10^{-1} \pm 0.01$	0.12 ± 0.01	-1.38 ± 0.01	3.17 ± 0.1	0.39 ± 0.01	40 ± 0.4



groups, while the $1,638 \text{ cm}^{-1}$ peak indicates the carbonyl group is present. The inhibitors adsorb on the metal surface and form a protective film that reduces biofilm formation and biocorrosion. XRD analysis reveals the presence of iron oxide-hydroxide, ferric oxide, and manganese oxide as the main corrosion products. In



a system with bacteria, stronger diffraction peaks indicate the bacteria's role in metal oxidation. However, samples treated with inhibitors show reduced peak intensities, indicating that the inhibitors effectively limit corrosion product formation. The halogen atoms in tetrabromo derivatives further enhance the inhibition efficiency by facilitating strong interactions with metal surface protection (El-Aouni et al., 2023), and the schematic representation of the proposed mechanism is shown in Figure 9. The synthesised inhibitors reduced the chemical corrosion as well in MIC. In conclusion, the synthesised organic inhibitor TBI is suitable for the carbon steel API 5LX80 in the crude oil reservoir.



Conclusion

This study demonstrated synthesised organic inhibitors TB-1,3-DOIBA, TB-1,3-DOIAA, and TB-1,3-DOIPA, which are effective and eco-friendly corrosion inhibitors with biocidal properties, which was suitable for mitigating the MIC on API 5LX80 carbon steel in a hypersaline (3.5 wt% NaCl) environment. This study revealed that TBI can act as a potential corrosion inhibitor with biocidal properties for carbon steel API 5LX80 in a hypersaline environment; it was enriched with corrosive bacteria. EIS analysis reveals that *P. aeruginosa* SKR10 accelerates the corrosion of carbon steel API 5LX80. The optimal antibacterial concentration of TBI was 200 ppm, which was obtained by the well diffusion method. EIS analysis confirmed that TBI formed a protective film on the metal surface and thus inhibited biofilm formation, and inhibition efficiencies were about 74%. On the basis of obtained results, TBI significantly inhibits corrosion due to biocidal properties. From these findings, the TBI inhibitor is expected to be favourable for the reducing risks of pipeline corrosion, oil reservoir, and biofouling and improves metal life span with negligible impact on the surrounding environment.

Data availability statement

The original contributions presented in the study are included in the article/supplementary material; further inquiries can be directed to the corresponding authors.

Author contributions

KV: conceptualization, data curation, methodology, and writing–original draft. SaS: conceptualization, methodology, and writing–original draft. MV: investigation, visualization, and writing–review and editing. SeS: writing–original draft

and methodology. JN: visualization and writing–review and editing. MA: resources, writing–review and editing. SD: formal analysis, validation, and writing–review and editing. PA: conceptualization, formal analysis, validation, and writing–review and editing. AR: project administration, supervision, validation, visualization, and writing–review and editing. TM: supervision and writing–review and editing.

Funding

The author(s) declare that financial support was received for the research, authorship, and/or publication of this article.

Acknowledgments

The authors are grateful to the Researchers Supporting Project no. (RSP2025R398), King Saud University, Riyadh, Saudi Arabia. The authors (MV and SeS) are grateful to the B S Abdur Rahman Crescent Institute of Science and Technology, Vandalur, Chennai-600048, for providing support and necessary facility.

Conflict of interest

The authors declare that the research was conducted in the absence of any commercial or financial relationships that could be construed as a potential conflict of interest.

Generative AI statement

The author(s) declare that no Generative AI was used in the creation of this manuscript.

Publisher's note

All claims expressed in this article are solely those of the authors and do not necessarily represent those of their affiliated

organizations, or those of the publisher, the editors and the reviewers. Any product that may be evaluated in this article, or claim that may be made by its manufacturer, is not guaranteed or endorsed by the publisher.

References

- Abdallah, Y., Shalabi, K., and Bayoumy, N. M. (2018). Eco-friendly synthesis, biological activity and evaluation of some new pyridopyrimidinone derivatives as corrosion inhibitors for API 5L X52 carbon steel in 5% sulfamic acid medium. *J. Mol. Struct.* 1171, 658–671. doi:10.1016/j.molstruc.2018.06.045
- AlSalhi, M. S., Devanesan, S., Rajasekar, A., and Kokilaramani, S. (2023). Characterization of plants and seaweeds based corrosion inhibitors against microbially influenced corrosion in a cooling tower water environment. *Arabian J. Chem.* 16 (3), 104513. doi:10.1016/j.arabjc.2022.104513
- Azzouzi, M. E., Azzaoui, K., Warad, I., Hammouti, B., Shityakov, S., Sabbahi, R., et al. (2022). Moroccan, Mauritania, and senegalese gum Arabic variants as green corrosion inhibitors for mild steel in HCl: weight loss, electrochemical, AFM and XPS studies. *J. Mol. Liq.* 347, 118354. doi:10.1016/j.molliq.2021.118354
- Batmanghelich, F., Li, L., and Seo, Y. (2017). Influence of multispecies biofilms of *Pseudomonas aeruginosa* and *Desulfovibrio vulgaris* on the corrosion of cast iron. *Corros. Sci.* 121, 94–104. doi:10.1016/j.corsci.2017.03.008
- Dou, W., Liu, J., Cai, W., Wang, D., Jia, R., Chen, S., et al. (2019). Electrochemical investigation of increased carbon steel corrosion via extracellular electron transfer by a sulfate reducing bacterium under carbon source starvation. *Corros. Sci.* 150, 258–267. doi:10.1016/j.corsci.2019.02.005
- El-Aouni, N., Dagdag, O., Amri, A. E., Kim, H., Dkhireche, N., Elbachiri, A., et al. (2023). Hybrid epoxy/Br inhibitor in corrosion protection of steel: experimental and theoretical investigations. *Environ. Sci. Pollut. Res.* 31 (1), 1033–1049. doi:10.1007/s11356-023-31171-7
- Gaines, R. H. (1910). Bacterial activity as a corrosive influence in the soil. *J. Industrial and Eng. Chem.* 2 (4), 128–130. doi:10.1021/ie50016a003
- Gu, T. (2014). Theoretical modeling of the possibility of acid producing bacteria causing fast pitting biocorrosion. *J. Microb. and Biochem. Technol.* 06 (02). doi:10.4172/1948-5948.1000124
- Ibrahim, H. A., Abdel-Latif, H. H., and Zaghoul, E. H. (2022). Phytochemical composition of *Avicennia marina* leaf extract, its antioxidant, antimicrobial potentials and inhibitory properties on *Pseudomonas fluorescens* biofilm. *Egypt. J. Aquatic Res.* 48 (1), 29–35. doi:10.1016/j.ejar.2021.10.007
- Idelftri, N. I. F., Dzulkifli, N. N., Ashari, N. A. N., Sapari, S., Razak, F. I. A., and Kungot, N. H. (2023). Synthesis, characterisation and corrosion inhibitory study of Meldrum's acid Thiosemicarbazone: weight Loss, SEM-EDX and DFT. *Inorg. Chem. Commun.* 150, 110485. doi:10.1016/j.inoche.2023.110485
- Jia, R., Tan, J. L., Jin, P., Blackwood, D. J., Xu, D., and Gu, T. (2018a). Effects of biogenic H₂S on the microbially influenced corrosion of C1018 carbon steel by sulfate reducing *Desulfovibrio vulgaris* biofilm. *Corros. Sci.* 130, 1–11. doi:10.1016/j.corsci.2017.10.023
- Jia, R., Yang, D., Al-Mahamedh, H. H., and Gu, T. (2017a). Electrochemical testing of biocide enhancement by a mixture of α -amino acids for the prevention of a corrosive biofilm consortium on carbon steel. *Industrial and Eng. Chem. Res.* 56 (27), 7640–7649. doi:10.1021/acs.iecr.7b01534
- Jia, R., Yang, D., Rahman, H. B. A., and Gu, T. (2018b). An enhanced oil recovery polymer promoted microbial growth and accelerated microbially influenced corrosion against carbon steel. *Corros. Sci.* 139, 301–308. doi:10.1016/j.corsci.2018.05.015
- Jia, R., Yang, D., Xu, J., Xu, D., and Gu, T. (2017b). Microbiologically influenced corrosion of C1018 carbon steel by nitrate reducing *Pseudomonas aeruginosa* biofilm under organic carbon starvation. *Corros. Sci.* 127, 1–9. doi:10.1016/j.corsci.2017.08.007
- Jung, I. G., Jeong, J. Y., Yum, S. H., and Hwang, Y. J. (2022). Inhibitory effects of selected medicinal plants on bacterial growth of methicillin-resistant *Staphylococcus aureus*. *Molecules* 27 (22), 7780. doi:10.3390/molecules27227780
- Kashyap, S. J., Sankannavar, R., and Dhu, G. (2022). Iron oxide (Fe₂O₃) synthesized via solution-combustion technique with varying fuel-to-oxidizer ratio: FT-IR, XRD, optical and dielectric characterization. *Mater. Chem. Phys.* 286, 126118. doi:10.1016/j.matchemphys.2022.126118
- Katara, G., Hemvani, N., Chitnis, S., Chitnis, V., and Chitnis, D. (2008). Surface disinfection by exposure to germicidal UV light. *Indian J. Med. Microbiol.* 26 (3), 241–242. doi:10.1016/s0255-0857(21)01870-3
- Kokilaramani, S., AlSalhi, M. S., Devanesan, S., Narenkumar, J., Rajasekar, A., and Govarthanan, M. (2020). Bacillus megaterium-induced biocorrosion on mild steel and the effect of Artemisia pallensmethanolic extract as a natural corrosion inhibitor. *Archives Microbiol.* 202 (8), 2311–2321. doi:10.1007/s00203-020-01951-7
- Kokilaramani, S., Narenkumar, J., AlSalhi, M. S., Devanesan, S., Obulisamy, P. K., Balagurunathan, R., et al. (2022). Evaluation of crude methanolic mangrove leaves extract for antibiofilm efficacy against biofilm-forming bacteria on a cooling tower wastewater system. *Arabian J. Chem.* 15 (7), 103948. doi:10.1016/j.arabjc.2022.103948
- Kokilaramani, S., Rajasekar, A., AlSalhi, M. S., and Devanesan, S. (2021). Characterization of methanolic extract of seaweeds as environmentally benign corrosion inhibitors for mild steel corrosion in sodium chloride environment. *J. Mol. Liq.* 340, 117011. doi:10.1016/j.molliq.2021.117011
- Lee, S. H., Glover, T., Lavey, N., Fu, X., Donohue, M., and Karunasena, E. (2024). Modified *in-vitro* AATCC-100 procedure to measure viable bacteria from wound dressings. *PLoS ONE* 19 (3), e0298829. doi:10.1371/journal.pone.0298829
- Li, M., Zhou, J., Li, Y., Zhu, G., Hu, Z., Liu, S., et al. (2024). Enhanced antibacterial and corrosion resistance of copper-containing 2205 duplex stainless steel against the corrosive bacterium *Shewanella* algae. *Bioelectrochemistry* 160, 108768. doi:10.1016/j.bioelechem.2024.108768
- Li, X. L., Narenkumar, J., Rajasekar, A., and Ting, Y. P. (2018). Biocorrosion of mild steel and copper used in cooling tower water and its control. *3 Biotech.* 8 (3), 178. doi:10.1007/s13205-018-1196-0
- Li, Y., Xu, D., Chen, C., Li, X., Jia, R., Zhang, D., et al. (2018). Anaerobic microbiologically influenced corrosion mechanisms interpreted using bioenergetics and bioelectrochemistry: a review. *J. Material Sci. Technol.* 34 (10), 1713–1718. doi:10.1016/j.jmst.2018.02.023
- Little, B., Blackwood, D., Hinks, J., Lauro, F., Marsili, E., Okamoto, A., et al. (2020). Microbially influenced corrosion—any progress? *Corros. Sci.* 170, 108641. doi:10.1016/j.corsci.2020.108641
- Liu, H., Gu, T., Asif, M., Zhang, G., and Liu, H. (2017). The corrosion behavior and mechanism of carbon steel induced by extracellular polymeric substances of iron-oxidizing bacteria. *Corros. Sci.* 114, 102–111. doi:10.1016/j.corsci.2016.10.025
- Liu, H., Gu, T., Zhang, G., Wang, W., Dong, S., Cheng, Y., et al. (2016). Corrosion inhibition of carbon steel in CO₂-containing oilfield produced water in the presence of iron-oxidizing bacteria and inhibitors. *Corros. Sci.* 105, 149–160. doi:10.1016/j.corsci.2016.01.012
- Liu, H., Xu, D., Dao, A. Q., Zhang, G., Lv, Y., and Liu, H. (2015). Study of corrosion behavior and mechanism of carbon steel in the presence of *Chlorella vulgaris*. *Corros. Sci.* 101, 84–93. doi:10.1016/j.corsci.2015.09.004
- Liu, J., Jia, R., Zhou, E., Zhao, Y., Dou, W., Xu, D., et al. (2018). Antimicrobial Cu-bearing 2205 duplex stainless steel against MIC by nitrate reducing *Pseudomonas aeruginosa* biofilm. *Int. Biodeterioration & Biodegrad.* 132, 132–138. doi:10.1016/j.ibiod.2018.03.002
- Majidi, H. J., Mirzaee, A., Jafari, S. M., Amiri, M., Shahrousvand, M., and Babaei, A. (2019). Fabrication and characterization of graphene oxide-chitosan-zinc oxide ternary nano-hybrids for the corrosion inhibition of mild steel. *Int. J. Biol. Macromol.* 148, 1190–1200. doi:10.1016/j.jbiomac.2019.11.060
- Moradi, M., Gao, Y., Narenkumar, J., Fan, Y., Gu, T., Carmona-Martinez, A. A., et al. (2024). Filamentous marine Gram-positive *Nocardiopsis dassonvillei* biofilm as biocathode and its electron transfer mechanism. *Sci. Total Environ.* 908, 168347. doi:10.1016/j.scitotenv.2023.168347
- Muthukrishnan, P., Jeyaprabha, B., and Rakash, P. (2017). Adsorption and corrosion inhibiting behavior of Lanneacoramandelic leaf extract on mild steel corrosion. *Arabian J. Chem.* 10, S2343–S2354. doi:10.1016/j.arabjc.2013.08.011
- Narenkumar, J., Elumalai, P., Subashchandrabose, S., Megharaj, M., Balagurunathan, R., Murugan, K., et al. (2019). Role of 2-mercaptopyridine on control of microbial influenced corrosion of copper CW024A metal in cooling water system. *Chemosphere* 222, 611–618. doi:10.1016/j.chemosphere.2019.01.193
- Narenkumar, J., Madhavan, J., Nicoletti, M., Benelli, G., Murugan, K., and Rajasekar, A. (2016). Role of bacterial plasmid on biofilm formation and its influence on corrosion of engineering materials. *J. Bio-Tribo-Corrosion* 2 (4), 24. doi:10.1007/s40735-016-0054-z
- Obot, I., Obi-Egbedi, N., and Umoren, S. (2009). Antifungal drugs as corrosion inhibitors for aluminium in 0.1M HCl. *Corros. Sci.* 51 (8), 1868–1875. doi:10.1016/j.corsci.2009.05.017
- Parthipan, P., AlSalhi, M. S., Devanesan, S., and Rajasekar, A. (2021). Evaluation of *Syzygium aromaticum* aqueous extract as an eco-friendly inhibitor for microbially influenced corrosion of carbon steel in oil reservoir environment. *Bioprocess Biosyst. Eng.* 44 (7), 1441–1452. doi:10.1007/s00449-021-02524-8

- Parthipan, P., Narenkumar, J., Elumalai, P., Preethi, P. S., Usha Raja Nanthini, A., Agrawal, A., et al. (2017). Neem extract as a green inhibitor for microbiologically influenced corrosion of carbon steel API 5LX in a hypersaline environment. *J. Mol. Liq.* 240, 121–127. doi:10.1016/j.molliq.2017.05.059
- Pinnock, T., Voordouw, J., and Voordouw, G. (2018). Use of carbon steel ball bearings to determine the effect of biocides and corrosion inhibitors on microbiologically influenced corrosion under flow conditions. *Appl. Microbiol. Biotechnol.* 102 (13), 5741–5751. doi:10.1007/s00253-018-8974-9
- Qi, R., Qian, C., and Wang, Y. (2024). Biofilm formation on MgFe-LDH@quartz sand as novel wetland substrate under varied C/N ratios for BDE-47 removal. *Environ. Pollut.* 124779. doi:10.1016/j.envpol.2024.124779
- Rajasekar, A., Anandkumar, B., Maruthamuthu, S., Ting, Y. P., and Rahman, P. K. S. M. (2009). Characterization of corrosive bacterial consortia isolated from petroleum-product-transporting pipelines. *Appl. Microbiol. Biotechnol.* 85 (4), 1175–1188. doi:10.1007/s00253-009-2289-9
- Rajasekar, A., Balasubramanian, R., and Vm Kuma, J. (2011). Role of hydrocarbon degrading bacteria *Serratiamarcescens* ACE2 and *Bacillus cereus* ACE4 on corrosion of carbon steel API 5LX. *Industrial and Eng. Chem. Res.* 50 (17), 10041–10046. doi:10.1021/ie200709q
- Rajput, A., Ramkumar, J., and Gondal, K. (2021). Cavitation resistance of a Cr-Mn stainless steel, A mild steel, and A high-carbon steel based on rust protectivity and corrosion behavior. *J. Mater. Eng. Perform.* 31 (1), 439–447. doi:10.1007/s11665-021-06162-9
- Sachan, R., and Singh, A. K. (2020). Comparison of microbial influenced corrosion in presence of iron oxidizing bacteria (strains DASEWM1 and DASEWM2). *Constr. Build. Mater.* 256, 119438. doi:10.1016/j.conbuildmat.2020.119438
- Salgar-Chaparro, S. J., Lepkova, K., Pojtanabuntoeng, T., Darwin, A., and &chuca, L. L. (2020). Microbiologically influenced corrosion as a function of environmental conditions: a laboratory study using oilfield multispecies biofilms. *Corros. Sci.* 169, 108595. doi:10.1016/j.corsci.2020.108595
- Salgar-Chaparro, S. J., Tarazona, J., and &chuca, L. L. (2022). Corrosion of carbon steel by *Shewanellachilikensis* DC57 Under Thiosulphate and nitrate reducing conditions. *Front. Bioeng. Biotechnol.* 10, 825776. doi:10.3389/fbioe.2022.825776
- Sethi, K. K., Vullo, D., Verma, S. M., Tanç, M., Carta, F., and &Supuran, C. T. (2013). Carbonic anhydrase inhibitors: synthesis and inhibition of the human carbonic anhydrase isoforms I, II, VII, IX and XII with benzene sulfonamides incorporating 4,5,6,7-tetrabromophthalimide moiety. *Bioorg. and Med. Chem.* 21 (19), 5973–5982. doi:10.1016/j.bmc.2013.07.044
- Su, H., Tang, R., Peng, X., Gao, A., and Han, Y. (2020). Corrosion behavior and mechanism of carbon steel influenced by interior deposit microflora of an in-service pipeline. *Bioelectrochemistry* 132, 107406. doi:10.1016/j.bioelechem.2019.107406
- Su, Y., Shi, Y., Li, Y., Zhao, X., Wan, H., Yu, H., et al. (2023). Corrosion behavior on carbon steel affected by iron-reducing bacteria via dissimilatory Fe(III) reduction in simulated marine atmospheric environment. *Corros. Sci.* 220, 111283. doi:10.1016/j.corsci.2023.111283
- Sun, Z., Madej, E., Genç, A., Muhler, M., Arbiol, J., Schuhmann, W., et al. (2016). Demonstrating the steady performance of iron oxide composites over 2000 cycles at fast charge-rates for Li-ion batteries. *Chem. Commun.* 52 (46), 7348–7351. doi:10.1039/c6cc00168h
- Swathi, K., Vajiravel, M., Kalishankar, B., Titas Kumar, M., Ayan, D., and Narayan, K. S. (2019). A solution processed ultrathin molecular dielectric for organic field-effect transistors. *ACS Appl. Electron. Mater.* 1 (4), 485–493. doi:10.1021/acsaem.8b00109
- Tagle, L. Z., Terraza, C. A., Tundidor-Camba, A., and Coll, D. (2015). Silicon-containing poly (esters) with halogenated bulky side groups. Synthesis, characterization and thermal studies. *RSC Adv.* 5, 49132–49142. doi:10.1039/C5RA06896G
- Usher, K., Kaksonen, A., Cole, I., and &rney, D. (2014). Critical review: microbially influenced corrosion of buried carbon steel pipes. *Int. Biodeterioration & Biodegrad.* 93, 84–106. doi:10.1016/j.ibiod.2014.05.007
- Vignesh, K., Sujithra, S., Vajiravel, M., Narenkumar, J., Das, B., AlSalhi, M. S., et al. (2024). Synthesis of novel N-substituted tetrabromophthalic as corrosion inhibitor and its inhibition of microbial influenced corrosion in cooling water system. *Sci. Rep.* 14 (1), 25408. doi:10.1038/s41598-024-76254-8
- Wang, D., Kijlka, P., Saleh, M. A., Kumseranee, S., Punpruk, S., and &Gu, T. (2022). Tafel scan schemes for microbiologically influenced corrosion of carbon steel and stainless steel. *J. Material Sci. Technol.* 130, 193–197. doi:10.1016/j.jmst.2022.05.018
- Wang, H., Ju, L. K., Castaneda, H., Cheng, G., and Newby, B. M. Z. (2014). Corrosion of carbon steel C1010 in the presence of iron oxidizing bacteria *Acidithiobacillusferrooxidans*. *Corros. Sci.* 89, 250–257. doi:10.1016/j.corsci.2014.09.005
- Wang, Z., Li, H., Xu, L., Liu, Q., Zha, L., and Lin, S. (2018). Electrochemical corrosion study of zircaloy-4 in a LIOH solution at high temperature and pressure. *Int. J. Electrochem. Sci.* 13 (12), 12163–12171. doi:10.20964/2018.12.20
- Wolodko, J., Haile, T., Khan, F., Taylor, C., Eckert, R., Hashemi, S. J., et al. (2018). Modeling of microbiologically influenced corrosion (MIC) in the oil and gas industry - past, present and future. *CORROSION*. Available at: <https://onepetro.org/NACECORR/proceedings/CORR18/All-CORR18/NACE-2018-11398/126151>.